CORROSION SCIENCE AND TECHNOLOGY, Vol.2, No.1(2003), pp.30~35

A Comparison of Corrosion Performance of Zirconium Grain Refined MEZ and AZ91 Alloys

Guangling Song and David StJohn

CRC for Cast Metals Manufacturing (CAST)
Department of Mining, Minerals and Materials Engineering,
The University of Queensland
Brisbane, QLD 4072, Australia

In this study, sand cast AZ91E and zirconium grain refined MEZ are representative of two typical groups of magnesium alloys: those containing aluminium and those containing no aluminium but with zirconium as a grain refiner. The corrosion performance of these two alloys was evaluated and compared in 5%wt NaCl solution through measurements of weight loss and polarisation curves and examination of microstructure. Corrosion damage of AZ91E was deeper and more localised than that of MEZ, while MEZ had a lower rate of cathodic hydrogen evolution and a higher rate of anodic dissolution than AZ91E. These differences in behaviour can be related to the differences in microstructure and chemical composition between the two alloys.

Keywords : *magnesium, corrosion, microstructure, zirconium grain refiner*

1. Introduction

Traditionally, magnesium alloys can be classified into two groups: 1) those containing aluminium as a primary alloying element, and 2) those free of aluminium and containing a small amount of zirconium for the purpose of grain-refinement.

The corrosion performance of the first group of alloys has been investigated, and aluminium is regarded as a beneficial element in improving corrosion resistance.[1),2),3)] AZ91 is a typical alloy of the first group, and has been widely used in practice. The purity of this alloy has a critical influence on its corrosion rate. By increasing purity, the corrosion rate can be significantly reduced. AZ91E is a high purity version of this alloy, and is normally used for sand castings.

For the second group of alloys, it is generally believed that the impurities, particularly iron and nickel, combine with zirconium and form insoluble precipitates, so the zirconium refined alloys are effectively "high purity".[4),5)] Thus, zirconium in this group of alloys is also a beneficial element in terms of corrosion performance. WE54 and WE43 are relatively popular zirconium-grain-refined alloys containing rare-earth elements. Recently, Magnesium Elektron (MEL) developed a new alloy (designated as MEZ) of the second group with satisfactory mechanical and creep properties after zirconium is added as a grain refiner. The corrosion resistance of this alloy has been measured[6)] to be lower than 1 mg/cm^2/day under the standard salt spray test (ASTM B117). This alloy also has low impurity levels similar to AZ91E.

The corrosion performance and mechanisms of these two groups of alloys have not been compared. In this study, AZ91E and MEZ were selected as representatives of these two groups of alloys, and their corrosion performance and mechanisms were compared.

2. Experimental

2.1 Specimens and solution

Two specimens were investigated: high purity sand cast AZ91E and zirconium grain refined sand cast MEZ_R. The compositions of the alloys are given in Table 1.

A 5 wt% NaCl solution was prepared according to ASTM B117 and used in all tests.

All potentials given in the paper are relative to the silver-silver chloride (saturated KCl) reference electrode and all experiments were carried out at 24±1 ℃.

2.2 Immersion and weight loss

Specimens were weighed, and each of them was hung in a beaker containing about 450 ml NaCl solution. After

Table 1. Composition of MEZ and AZ91 in weight percent except Fe, Cu and Ni in ppm

Elements	AZ91E, wt%	MEZ_R, wt%
Al	9.13	0.03
Zn	0.88	0.42
Zr	<0.002	0.60
Mn	0.23	0.11
Fe	50ppm	40ppm
Ni	<20ppm	<20ppm
Cu	90ppm	<50ppm
Ce	<0.002	1.28
Nd	<0.002	0.37
Pr	<0.002	0.09
La	<0.02	0.65
Other elements	<0.005	<0.005
Mg	Remainder	Remainder

about 5 days of immersion, the specimens were quickly cleaned with water and the loose corrosion products on the specimen surfaces were removed with a nylon brush. They were then immersed in chromic acid (200 g/L CrO_3 +10 g/L $AgNO_3$) for about 5-10 minutes to further remove the corrosion products that could not be brushed off. After the specimens were washed with water, they were dried and weighed again. The difference between the original and final weights was recorded as the weight loss caused by corrosion.

2.3 Metallography

The specimens were polished and etched in 2% nital solution to reveal the microstructure and the phases present. They were then immersed horizontally in the salt solution, about 1 mm below the surface of the solution. An optical microscope was mounted over the solution directly above the specimens. The corrosion process of each specimen was observed in situ during immersion by the optical microscope. After about 3~4 hours. The samples were then quickly washed with alcohol and dried. The corroded specimens were further investigated under an optical microscope.

2.4 Corrosion potential

The specimens were properly sealed with epoxy resin, leaving 1 x 1 cm^2 unsealed areas exposed for electrochemical measurements. They were immersed in the solution and their corrosion potentials were measured using a Solartron potentiostat Model 1287.

2.5 Polarisation curves

The specimens that were used in the measurement of corrosion potential were immersed in an electrolytic cell containing the solution. Polarisation curves were obtained using the potentiostat at a scanning rate of 10 mV/min.

2.6 Hydrogen evolution collection

Specimens prepared in the same manner as those used in the measurement of polarisation curves were put into an electrolytic cell. A constant current was applied to the samples by the Solartron potentiostat while a funnel over the specimen captured all gas bubbles arising from the specimen surface into a burette which was full of the solution and mounted vertically over the funnel. The entry of hydrogen displaced the solution in the burette, so the volume of hydrogen generated from the specimen was measured by recording the displaced solution volumes.

3. Results and discussion

3.1 Corrosion performance

The results of weight loss are presented in Table 2. Both AZ91E and MEZ_R have a low corrosion rate under the salt immersion condition. The weight loss rate of AZ91E is about half of the MEZ_R, ie, AZ91E is more corrosion resistant than MEZ_R.

Table 2. Weight loss rates of MEZ and AZ91

	Weight loss rate-1 ($mg/cm^2/day$)	Weight loss rate-2 ($mg/cm^2/day$)	Weight loss rate-3 ($mg/cm^2/day$)	Average weight loss rate ($mg/cm^2/day$)
AZ91E	0.889	0.914	1.090	0.964
MEZR	1.996	2.012	2.025	2.011

The difference in the corrosion rate can be confirmed by the corrosion morphologies of these two alloys after immersion (Fig. 1). Most of the surface area of MEZ_R was corroded after 5 days of immersion while the corrosion of AZ91E only occurred on part of surface area. In the corroded areas, AZ91E and MEZ_R have different appearances. Higher magnification photographs of the corrosion areas shown in Fig. 2 exhibit many deep pits that were formed in the corroded areas on AZ91E during the immersion corrosion test, whilst the depth of the corroded areas on MEZ_R was relatively shallow and uniform.

3.2 Electrochemical behaviour

AZ91E had a higher corrosion potential than MEZ_R (see Fig. 3). The corrosion potential of AZ91E initially dec

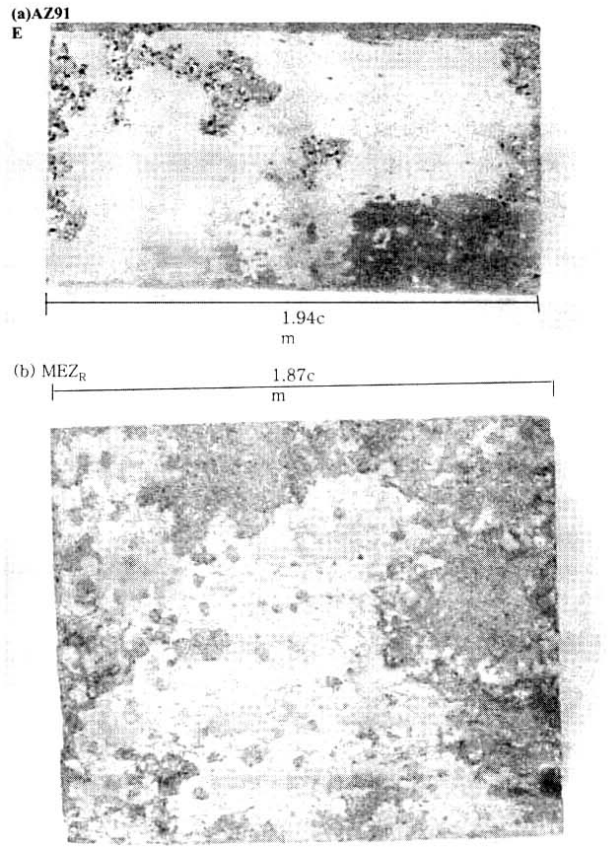

Fig. 1. Corrosion morphologies of (a) AZ91E and (b) MEZ_R after 5 days of immersion in 5% NaCl solution at room temperature [s1]

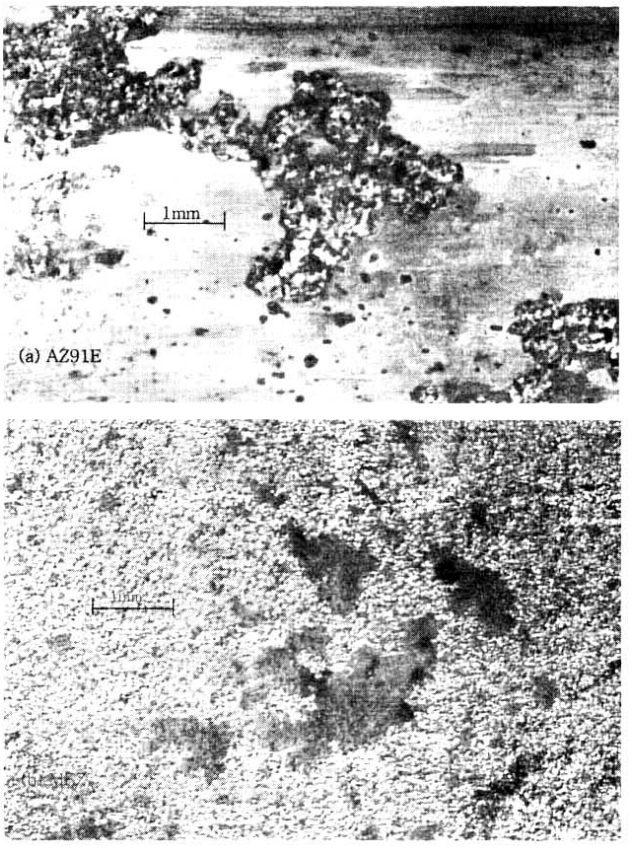

Fig. 2. Detailed corrosion patterns of (a) AZ91E and (b) MEZ_R after 5 days of immersion in 5% NaCl solution at room temperature

reased with time until some pits were formed and hydrogen bubbles evolved from the pits became visible. The corrosion potential of MEZ_R, on the contrary, always increased with time from the beginning until it stabilised around -1.62V. At that moment, black corroded areas had appeared on the electrode surface, and hydrogen evolution from these corroded areas was observed.

The corrosion potential of an electrode is normally governed by anodic and cathodic reactions on this electrode. A decrease in corrosion potential results from a faster increasing rate of anodic reaction than that of the cathodic reaction or a faster decreasing rate of cathodic reaction than that of the anodic reaction. On the other hand, a more rapid decreasing rate of anodic reaction or a swifter increasing rate of cathodic reaction results in an increasing corrosion potential.

In this study, it was observed that the rate of hydrogen evolution from AZ91E and MEZ_R both increased with time. Therefore, the increase of the corrosion potential of MEZ_R could be mainly ascribed to increasing hydrogen evolution, while the deceasing corrosion potential of

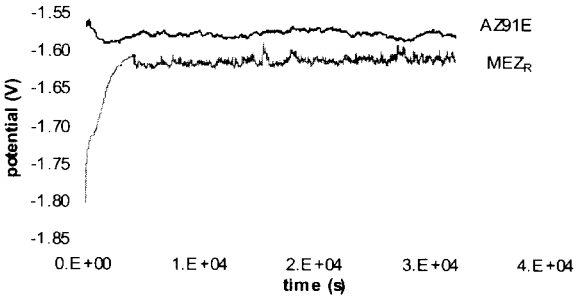

Fig. 3. Change in corrosion potential of AZ91E and MEZ_R in 5% NaCl solution

AZ91E could result from increasing anodic dissolution of magnesium. These proposed causes of the variation of the corrosion potentials of AZ91E and MEZ_R can be proven by examining cyclically scanned polarisation curves (Fig. 1).

Forward scanning of the polarisation curves started from a cathodic potential where the surfaces of the alloys were not corroded. On the forward scanned curves, the corrosion potential of AZ91E is about -1.56V and that of MEZ_R

-1.68V, the latter being higher than the former. This is consistent with the corrosion potentials of these two alloys at the beginning of immersion when their surfaces were not significantly corroded as is shown in Fig. 3. On the backward scanned curves, the corrosion potential of AZ91E shifted to a more negative value and the corrosion potential of MEZ_R became less negative. These are in coincidence with the measured potentials in Fig. 3. This is because during backward scanning, the surfaces of the alloys were severely corroded, thus the corrosion potentials, to some extent, correspond to the potentials of the alloys after being immersed in solution for a long time as shown in Fig. 3.

The most significant feature of Fig. 4 is the difference between forward and backward scanned curves. For AZ91E, there was no significant difference between the forward and backward scanned curves in the cathodic region, whilst the backward scanned curve in the anodic region is much higher than the forward scanned curve. This supports the above statement that the anodic shift of the corrosion potential is due to the dramatically increased anodic dissolution of AZ91E. Fig. 4 also shows that the backward scanned curve for MEZ_R is higher than the forward scanned curve in both anodic and cathodic regions. However, compared with AZ91E, the increase in the anodic region is not significant, but much more significant in the cathodic region. This proves the hypothesis that the increase in the corrosion potential of MEZ_R was caused by a more rapid increase in hydrogen evolution.

In addition, MEZ_R has a slower rate of cathodic hydrogen evolution than AZ91E, whereas the anodic dissolution of AZ91E is much faster than that of MEZ_R (Fig. 4). At the same potentials, hydrogen evolution is much easier and the dissolution of magnesium is much more difficult for AZ91E than for MEZ_R.

The results of the measurement of hydrogen evolution further verify the postulation that AZ91E has a slower anodic dissolution rate than MEZ_R during corrosion (Table 3). At the corrosion potentials, the measured hydrogen volume from MEZ_R is larger than that from AZ91E. This is a reasonable result, as at the corrosion potential the rate of anodic dissolution of a magnesium alloy is equal to the rate of hydrogen evolution.[7] Under an anodic polarisation current density, the rate of anodic dissolution of a magnesium alloy should be equal to the rate of hydrogen evolution plus the applied current. Hence, under the same anodic current, the measured hydrogen volume reflects the total amount of anodically dissolved magnesium alloy. Therefore, in Table 3 the larger measured volume of hydrogen from MEZ_R than from AZ91E under the anodic polarisation current density suggests that anodic dissolution of MEZ is faster than that of AZ91E.

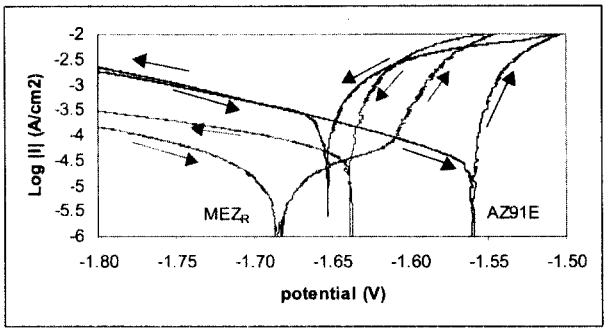

Fig. 4. Cyclically scanned polarisation curves of AZ91E and MEZ_R

Table 3. Volume of hydrogen evolved from AZ91E and MEZ_R at their corrosion potentials and under an anodic polarisation current density of 0.5 mA/cm^2

	At corrosion potential (I=0)	Anodically polarised (I=0.5 mA/cm^2)
AZ91E	1.9 ml	9.5 ml
MEZ_R	4.0 ml	14.2 ml

3.3 Composition and microstructure

According to Table 1, AZ91E and MEZ_R are similar in impurity levels and manganese content. So, the influences of the impurities and manganese on the corrosion performance of these two alloys can be neglected. The meaningful difference in composition between these two alloys is that AZ91 contains considerably higher levels of aluminium and zinc than MEZ_R, whilst MEZ_R has a small amount of zirconium and rare-earth elements. The difference in composition of these two alloys led to different microstructures that could play an important role in the corrosion of these two alloys.

Fig. 5 and Fig. 6 show the microstructures of the two alloys during corrosion and after corrosion. The original microstructures of these two alloys are still visible in the uncorroded areas. MEZ_R has a smaller grain size than AZ91E. Also, the volume fraction of intergranular RE-phases in MEZ_R is much less than that of $Mg_{17}Al_{12}$ (β) present in AZ91E. For AZ91E (Fig. 5), the β phase is present in two forms: β layers on the grain boundaries that are formed as part of a divorced eutectic and a lamellar-like structure which is formed by discontinuous precipitation. Hydrogen evolution took place on the edges of the β phase, as indicated by the arrow in Fig. 5 (a). The β phase (including the eutectic and discontinuously precipitated β) did not corrode (Fig. 5 (b)). Corrosion only occurred in the α phase. In many cases, corrosion appeared

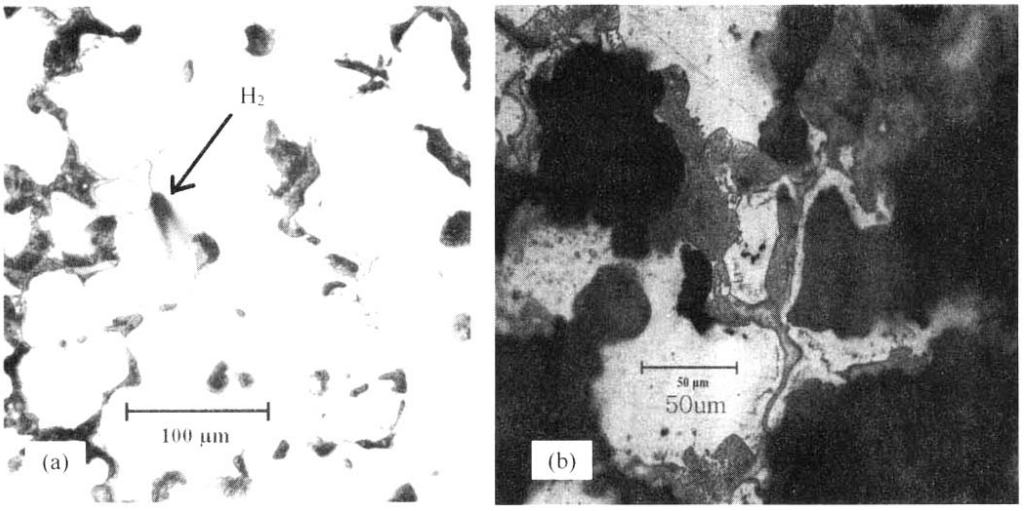

Fig. 5. Microstructures of AZ91E (a) during and (b) after corrosion in 5% NaCl solution

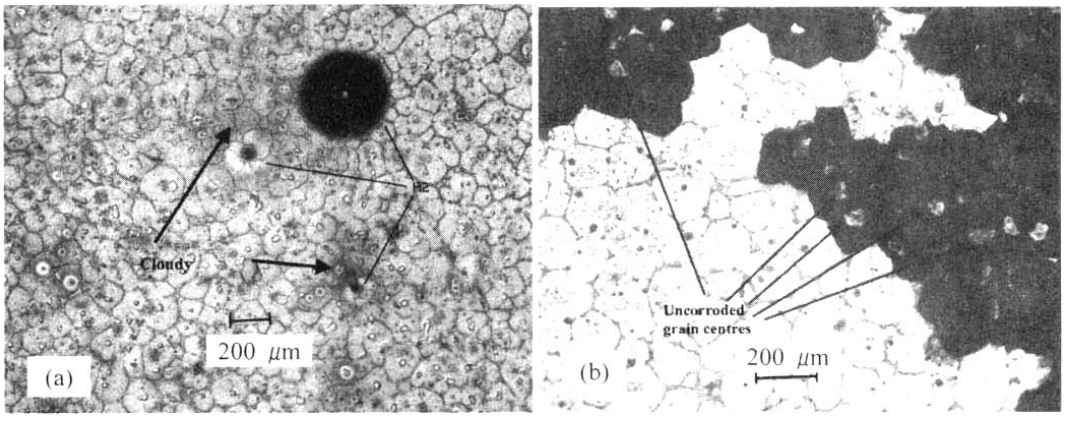

Fig. 6. Microstructures of MEZ_R (a) during and (b) after corrosion in 5% NaCl solutio

to be stopped by the β phase in the grain boundaries. However, careful examination revealed that corrosion had actually stopped before it reached the β phase.

The microstructure of MEZ_R (Fig. 6) is characterised by equiaxed primary grains separated by the eutectic boundary phase. It has been identified[8] that the primary grains are magnesium solid solution depleted in rare earths, whilst the grain boundary phase is a rare earth based intermetallic. Within the matrix, there are some tiny precipitates. Cathodic hydrogen evolution is from particular sites in the grains. These sites do not enlarge or spread out with time. They are inert cathodic phases in the alloy. The corrosion of MEZ_R appears to be mostly confined within grains by the RE boundary phase, and many central areas of the grain remain uncorroded (Fig. 6(b)). The boundary phase is corrosion resistant. It remains intact even in the corroded areas.

A comparison between the microstructures reveals significant differences in corrosion behaviour and anodic and cathodic processes between these two alloys. The β phase is active in cathodic hydrogen evolution in AZ91E,[9] whereas cathodic hydrogen is difficult to evolve from the grain boundary phase in MEZ_R (it can only be released from a limited number of particles in the alloy). Therefore, AZ91E has a higher cathodic polarisation curve than MEZ_R.

In AZ91E, not only can the β phase stop corrosion, but the grain boundary zones which are rich in aluminium[10] also act as barriers to corrosion. It has been reported[11] that α phase with a high content of aluminium would exhibit a passivating trend. The passivating trend would retard the anodic dissolution process. Although the rare-earth elements and zirconium have a beneficial effect on the corrosion resistance of MEZ_R,[12] their contents are much lower than the amount of aluminium in AZ91E. Thus the RE and zirconium could not influence the

corrosion resistance as significantly as aluminium. There fore, AZ91E has a lower anodic dissolution rate than MEZ_R.

The corrosion on MEZ_R was mainly confined by the grain boundary phase, so that the corroded areas follow the shapes of grains. In AZ91E, the aluminium rich zones are mainly adjacent to the β phase that is irregularly distributed, and the grains are much coarser. The corroded areas follow the irregular zones which are depleted in aluminium, then penetrate until it approaches an aluminium rich barrier at the bottom of the grain. As a result, AZ91E has deeper and more localised corroded areas than MEZ_R.

4. Conclusions

1) Based on weight loss, hydrogen evolution and polarisation behaviour, AZ91E is slightly more corrosion resistant than MEZ_R in 5% NaCl, but the corrosion of AZ91E is more localised and penetrates deeper than MEZ_R.

2) MEZ_R has a lower rate of cathodic hydrogen evolution than AZ91E, whilst anodic dissolution of AZ91E is slower than that of MEZ_R.

3) The β phase in AZ91E is probably responsible for the higher rate of cathodic hydrogen evolution, and the high aluminium content could be the main reason for the lower rate of anodic dissolution of AZ91E. Coarser grains and an irregular distribution of aluminium constrained the corrosion, so that the corroded areas in A91E are deep and localised.

4) The cathodically inactive grain boundary phase in MEZ_R led to a low rate of cathodic hydrogen evolution. A fine and uniform distribution of the grains in MEZ_R made the corrosion of MEZ_R relatively uniform and shallow.

Acknowledgment

The authors thank Mr. Zhiming Shi and Mr. Gary Cleeland for their assistance in electrochemical and corrosion tests. The support of a start-up fund from the University of Queensland is also acknowledged. CAST was established under and is supported by the Australian Government's Cooperative Research Centres Program.

References

1. O. Lunder, K. Nisancioglu, and R. S. Hansen, "Corrosion of Die Cast Magnesium-Aluminum Alloys", SAE Technical Paper Series#930755, Detroit, (1993).
2. G. L. Makar and K. Kruger, *J. Electrochem. Soc.*, **137**, 414 (1990).
3. C. B. Baliga and P. Tsakiropoulos, *Materials Science and Technology*, **9**, 513 (1993).
4. E. F. Emley, "Principles of Magnesium Technology", Chapter XX, (1966).
5. D. S. Tawil, "Protection of Magnesium Components in Military Applications", Paper No. 90445, NACE '90 Conference, Las Vegas, (1990)
6. G. Song and D. StJohn, "The Effect of Zirconium Grain Refinement on the Corrosion Behaviour of Magnesium-Rare Earth Alloy MEZ", CAST Report
7. G. Song and D. StJohn, "An hydrogen evolution method for the estimation of the corrosion rate of magnesium alloy", John N. Hryn, ed. Magnesium Technology 2001, TMS pp.255-262 (2001).
8. C. J. Bettles and C. T. Forwood (compiled), "Identification of a Creep Resistant Magnesium Alloy for the Manufacture of Engine Blocks" CAST internal confidential report. (1998).
9. G. Song, A. Atrens, X. Wu, and B. Zhang, *Corrosion Science*, **40**(10), 1769 (1998).
10. M. Dargusch, "Elevated temperature deformation of diecast Mg alloy AZ91D", in G. W. Lorimer (ed), "Proceedings of the Third International Magnesium Conference", Manchester, UK, April,1996, pp.153-165
11. O. Lunder, J. E. Lein, T. Kr. Aune, and K. Nisancioglu, *Corrosion*, **45**(9), 741.
12. I. Nakatsugawa, S. Kamado, Y. Kojima, R. Ninomiya, and K. Kubota, "Corrosion Behaviour of Magnesium Alloys Containing Heavy Rare Earth Elements", in G.W.Lorimer (ed) "Proceedings of the Third International Magnesium Conference", Manchester, pp.687-698, (1996).